COMPOSITE WESENHEIT BASED GALACTIC BVIJHK LEAVITT LAW CALIBRATION

Shubham Mamgain[1,2]

[1] *Institute of Physics and Astronomy, University of Potsdam*
[2] *Dwarf Galaxy and Galactic Halo, AIP Potsdam*

17.11.2025

Abstract

Extragalactic distance measurement relies critically on the Cepheid period–luminosity relation, yet luminosity-based distances are significantly affected by interstellar extinction, introducing a three-fold uncertainty: Luminosity-Reddening-Distance. Using the total-to-selective absorption ratio, composite Wesenheit magnitudes constructed for $BVIJHK$ photometry of Galactic Cepheids to minimize reddening effects. Fouqué's extinction law is recalibrated to yield near-zero offsets between apparent and true Wesenheit magnitudes across fifteen color combinations at $R_V^{BV} = 3.23$. Adjusted extinction law is then used to determine $BVIJHK$ extinctions for 109 Galactic Cepheids with available Fernie reddenings and IRSB-based distances. Using refined reddening ratios and a prepared dataset, the distance–reddening calibration is performed by correlating the residuals of the Leavitt Laws with the corresponding residuals of the Wesenheit Leavitt Law. Metallicity effects are not considered in this study.

Two step calibration: First step focuses on distance calibration, $IJHK$ Period-Luminosity (PL) residuals are correlated with the corresponding Period-Wesenheit (PW) residuals, excluding the B and V bands, in order to resolve the degeneracy between band-dependent extinction and band-independent distance uncertainties. The infrared Wesenheit index $(I - H)$ is used in this initial step. A star-by-star adjustment of the distance modulus is performed to minimize the dispersion in reddening across bands, resulting in a distance-reddening correction pair for each individual Cepheid. After applying the first-order corrections to the input data, the procedure is repeated for the $BVIJ$ bands to derive more accurate reddening corrections, using the Wesenheit color $(V - J)$. The final corrections are then applied to derive the $BVIJHK$ Leavitt Laws, which are verified using 17 cluster Cepheids. For comparison, Gaia parallax-based Leavitt Laws are also derived for the same set stars.

Calibrated Leavitt Laws - I: Distance II: Reddening					
Band	**Scatter**	**Slope**	**(error)**	**Intercept**	**(error)**
76 Galactic Cepheids IRSB I: (I-J) and II: (H-K)					
B	$(0.045)_\sigma$	-1.885	($\pm$ 0.019)	-3.102	($\pm$ 0.005)
V	$(0.033)_\sigma$	-2.281	($\pm$ 0.014)	-3.911	($\pm$ 0.004)
I	$(0.034)_\sigma$	-2.581	($\pm$ 0.015)	-4.691	($\pm$ 0.004)
J	$(0.016)_\sigma$	-2.799	($\pm$ 0.007)	-5.177	($\pm$ 0.002)
H	$(0.015)_\sigma$	-2.931	($\pm$ 0.006)	-5.552	($\pm$ 0.002)
K	$(0.005)_\sigma$	-2.981	($\pm$ 0.002)	-5.613	($\pm$ 0.001)
71 Galactic Cepheids Gaia I: (V-K) and II: (H-K)					
B	$(0.056)_\sigma$	-1.954	($\pm$ 0.025)	-3.100	($\pm$ 0.007)
V	$(0.019)_\sigma$	-2.343	($\pm$ 0.009)	-3.908	($\pm$ 0.002)
I	$(0.028)_\sigma$	-2.640	($\pm$ 0.013)	-4.690	($\pm$ 0.003)
J	$(0.013)_\sigma$	-2.860	($\pm$ 0.006)	-5.174	($\pm$ 0.002)
H	$(0.008)_\sigma$	-2.988	($\pm$ 0.004)	-5.549	($\pm$ 0.001)
K	$(0.011)_\sigma$	-3.039	($\pm$ 0.005)	-5.609	($\pm$ 0.001)
29 LMC IRSB I: (I-K)					
V	$(0.053)_\sigma$	-2.705	($\pm$ 0.027)	14.296	($\pm$ 0.011)
I	$(0.032)_\sigma$	-2.959	($\pm$ 0.016)	13.604	($\pm$ 0.006)
J	$(0.017)_\sigma$	-3.123	($\pm$ 0.009)	13.215	($\pm$ 0.004)
K	$(0.027)_\sigma$	-3.224	($\pm$ 0.014)	12.783	($\pm$ 0.005)
32 SMC IRSB I: (V-J)					
V	$(0.028)_\sigma$	-2.865	($\pm$ 0.016)	15.174	($\pm$ 0.006)
I	$(0.031)_\sigma$	-3.093	($\pm$ 0.018)	14.369	($\pm$ 0.007)
J	$(0.029)_\sigma$	-3.020	($\pm$ 0.016)	13.800	($\pm$ 0.006)
K	$(0.035)_\sigma$	-3.264	($\pm$ 0.020)	13.369	($\pm$ 0.008)

Result: Gold dataset of 76 Cepheids, with first-order calibration in $(I - J)$ and second-order calibration in $(H - K)$, yields the Galactic Leavitt Laws as follows.

The distance moduli to the Magellanic Clouds, from $VIJK$ photometry, are estimated to be 18.322 ± 0.089 mag for the Large Magellanic Cloud (LMC) and 19.025 ± 0.056 mag for the Small Magellanic Cloud (SMC).

Description of Mathematical Notations			
Symbol	Description	Symbol	Description
m_λ	Apparent Magnitude	α_λ	Period Luminosity Slope
μ	Distance Modulus	γ_λ	Period Luminosity Intercept
M_λ	Absolute Magnitude	ΔW^{12}_λ	Period Wesenheit Residuals
E_{BV}	Interstellar Reddening	α^{12}_λ	Period Wesenheit Slope
A_λ	Interstellar Extinction	γ^{12}_λ	Period Wesenheit Intercept
R^{12}_λ	Total-to-selective Absorption	$\rho^{12}_{\kappa\lambda}$	Residual Correlation Slope
M^0_λ	True Absolute Magnitude	$\Delta^{12}_{\kappa\lambda}$	PL-PW Correlation Residuals
W^{12}_λ	Wesenheit Magnitude	$\delta A^{12}_{\kappa\lambda}$	Extinction Correction
ΔM_λ	Period Luminosity Residuals	$\delta E^{12}_{\kappa\lambda}$	Reddening Correction

1. Definitions

1.1 Distance, Reddening and Luminosity

Luminosity represents the measured photon flux received within a specific wavelength band, here corresponding to the $BVIJHK$ bands. The light emitted by a star, characterized by its intrinsic absolute magnitude M_λ^0, travels over large distances μ and undergoes extinction A_λ as it passes through the interstellar medium (ISM) before reaching the observer's detector with the observed intensity m_λ.

In this framework, the relation for the observed apparent magnitude can be expressed as:

$$m_\lambda = \mu + A_\lambda + M_\lambda^0 \tag{1}$$

where m_λ is the apparent magnitude in a given band λ, M_λ^0 is the intrinsic absolute magnitude, μ is the distance modulus, and A_λ is the interstellar extinction in that band.

On the right-hand side, the first term represents the distance modulus, μ. For computational convenience, distances measured in parsecs are converted into dimensionless logarithmic units, expressed in magnitudes. The distances for the 109Galactic Cepheids in the dataset are determined using two independent methods: (i) the Infrared Surface Brightness (IRSB) method Storm et al. (2011), and (ii) parallax measurements from *Gaia* DR3 Gaia Collaboration (2023). In this report, calibration is done for Gaia distances.

$$\mu = 5 \log D[pc] - 5$$

The interstellar medium (ISM) scatters, absorbs, and emits photons depending on the chemical composition, size, and abundance of its constituent particles, thereby imprinting characteristic signatures on the light spectrum at specific frequencies (or wavelengths). The reduction in light intensity within a given band due to these interactions with the ISM is referred to as *interstellar extinction*.

$$A_\lambda = m_\lambda - m_\lambda^0$$

The wavelength-dependent extinction for each individual Cepheid is determined from the measurement of the color excess, E_{BV}, along the line of sight Fernie (1995). Using the visual Galactic reddening ratio, $R_V = 3.23$ Sandage et al. (2004), within the framework of the Galactic extinction law, A_λ/A_V Fouqué et al. (2007), the interstellar extinction for the $BVIJHK$ bands can be estimated as follows:

$$A_\lambda = \frac{A_\lambda}{A_V} \times R_V \times E_{BV}$$

Here, the final factor, the color excess E_{BV}, quantifies the relative extinction difference between two photometric bands. In other words, it can also be expressed as the deviation of the observed color index $(B-V)$ from the intrinsic (or 'true') color index $(B-V)_0$:

$$\begin{aligned} E_{BV} &= (B-V) - (B-V)_0 \\ &= (B-B_0) - (V-V_0) \\ &= A_B - A_V \end{aligned}$$

The intermediate factor, the reddening ratio $R_V = A_V/E_{BV}$, represents the extinction-to-reddening ratio in the visual band. In the most general form, if the color excess between two bands is defined as $E_{12} = A_{m_1} - A_{m_2}$, then the corresponding reddening ratio can be expressed as:

$$R_\lambda^{12} = A_\lambda / E_{12}$$

Color excess from one combination of bands E_{12} can be transformed into any other bands combination as follows:

$$\begin{aligned} E_{12} &= A_1 - A_2 \\ &= R_1^{BV} * E_{BV} - R_2^{BV} * E_{BV} \\ &= (R_1^{BV} - R_2^{BV}) * E_{BV} \end{aligned}$$

This leads the transformation law for reddening ratio R:

$$R_\lambda^{12} = \frac{R_\lambda^{BV}}{R_1^{BV} - R_2^{BV}}$$

The values of R_λ^{BV} are calculated using extinction law as mentioned in Table 1.

$$R_\lambda^{BV} = \frac{A_\lambda}{A_V} \times R_V^{BV}$$

1.2 Wesenheit Magnitude

Since the reddening ratio, R_λ^{12}, quantifies the effect of the interstellar medium on the incoming light, it can be used to define a reddening-free magnitude corresponding to the star's true absolute magnitude Madore (1982). This relation can be expressed as:

$$\begin{aligned} R_\lambda^{12} &= A_\lambda / E_{12} \\ &= \frac{m_\lambda - m_\lambda^0}{(m_1 - m_2) - (m_1 - m_2)_0} \end{aligned}$$

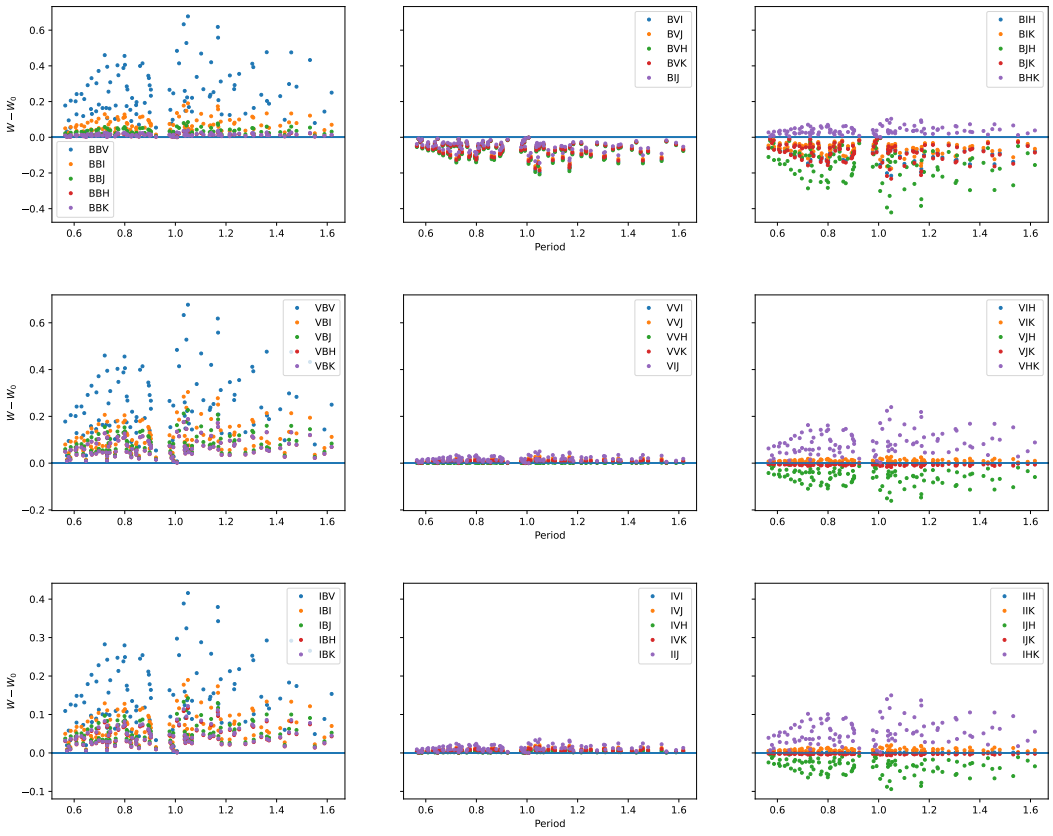

Figure 1: For BVI photometry, the deviation between apparent Wesenheit magnitude and absolute Wesenheit magnitude for all the color combination indicates a potential error in the reddening law.

On rearranging the terms, one can get the Wesenheit function W_λ^{12} corresponding to color $m_1 - m_2$.

$$m_\lambda - R_\lambda^{12}(m_1 - m_2) = m_\lambda^0 - R_\lambda^{12}(m_1 - m_2)_0 \tag{2}$$

$$W_\lambda^{12} = W_0 \tag{3}$$

This implies that, if R is accurately known, the apparent Wesenheit magnitude and the absolute Wesenheit magnitude should be identical. Here, we test the validity of this claim by comparing the deviations between the two versions of the Wesenheit magnitudes, where R is derived from the Fouque extinction law as given in Table 1.

This deviation in wesenheit $W - W_0$ would be zero, when following equality would be satisfying:

$$\delta A_\lambda - R_\lambda \delta E_{BV} - \delta R E_{BV} = 0 \tag{4}$$

Considering the last term of the above equation, Fouqué et al. (2007) extinction law have been adjusted to achieve minimum deviation in the wesenheit magnitudes.

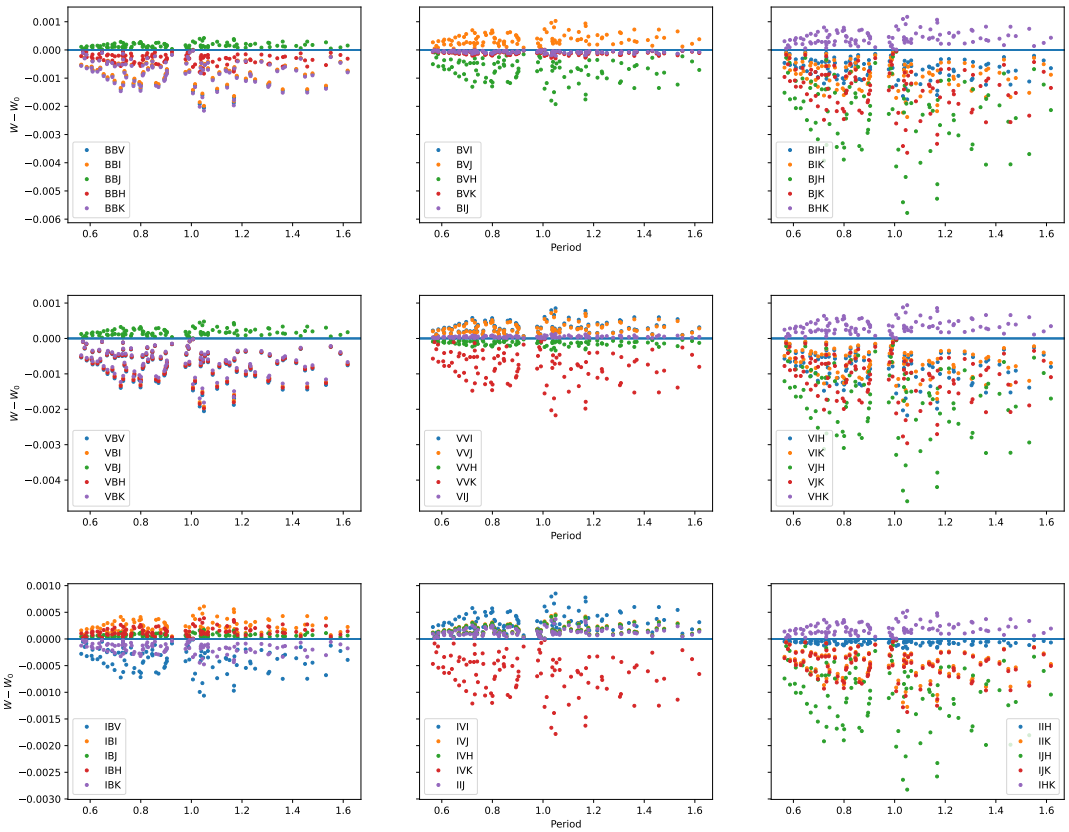

Figure 2: With the adjusted Fouqué extinction law, the deviation between the apparent and absolute Wesenheit magnitudes is reduced by a factor of ten.

After fine-tuning the Fouqué extinction law for our dataset, R_λ is assumed to be accurately known to the required precision, eliminating the last term in the above equation.

Table 1: Reddening Ratio metrics for composite photometry.

Extinction Law Fouqué et al. (2007)										
A_B^V	1.31	A_V^V	1.0	A_I^V	0.608	A_J^V	0.292	A_H^V	0.181	A_K^V	0.119
Adjusted Extinction Law										
A_B^V	1.2574	A_V^V	1.0	A_I^V	0.609	A_J^V	0.2967	A_H^V	0.1816	A_K^V	0.1231
Reddening Ratio calculated using $R_V^{BV} = 3.23$										
R_B^{12}		R_V^{12}		R_I^{12}		R_J^{12}		R_H^{12}		R_K^{12}	
BBV	4.887	VBV	3.887	IBV	2.367	JBV	1.153	HBV	0.706	KBV	0.478
BBI	1.94	VBI	1.543	IBI	0.939	JBI	0.458	HBI	0.28	KBI	0.19
BBJ	1.309	VBJ	1.041	IBJ	0.634	JBJ	0.309	HBJ	0.189	KBJ	0.128
BBH	1.169	VBH	0.93	IBH	0.566	JBH	0.276	HBH	0.169	KBH	0.114
BBK	1.108	VBK	0.882	IBK	0.537	JBK	0.262	HBK	0.16	KBK	0.108
BVI	3.216	VVI	2.557	IVI	1.557	JVI	0.759	HVI	0.464	KVI	0.315
BVJ	1.788	VVJ	1.422	IVJ	0.866	JVJ	0.422	HVJ	0.258	KVJ	0.175
BVH	1.537	VVH	1.222	IVH	0.744	JVH	0.363	HVH	0.222	KVH	0.15
BVK	1.434	VVK	1.14	IVK	0.694	JVK	0.338	HVK	0.207	KVK	0.14
BIJ	4.025	VIJ	3.201	IIJ	1.95	JIJ	0.95	HIJ	0.581	KIJ	0.394
BIH	2.943	VIH	2.341	IIH	1.425	JIH	0.694	HIH	0.425	KIH	0.288
BIK	2.587	VIK	2.057	IIK	1.253	JIK	0.61	HIK	0.374	KIK	0.253
BJH	10.947	VJH	8.706	IJH	5.302	JJH	2.583	HJH	1.581	KJH	1.071
BJK	7.24	VJK	5.758	IJK	3.506	JJK	1.708	HJK	1.046	KJK	0.708
BHK	21.376	VHK	17.0	IHK	10.353	JHK	5.044	HHK	3.087	KHK	2.091
LMC Extinction Law with $R_V = 3.4$ Wang & Chen (2023)										
A_B^V	1.32	A_V^V	1.0	A_I^V	0.65	A_J^V	0.30	A_H^V	0.20	A_K^V	0.15
SMC Extinction Law with $R_V = 2.53$										
A_B^V	1.40	A_V^V	1.0	A_I^V	0.7	A_J^V	0.38	A_H^V	0.28	A_K^V	0.2

1.3 Error Contribution in Absolute and Wesenheit magnitude

Following are the definitions of 'true' absolute magnitude and wesenheit magnitude for color (B-V):

$$M_\lambda^0 = m_\lambda - R_\lambda^{BV} * E(B-V) - \mu \tag{5}$$

$$W_\lambda^{BV} = m_\lambda - R_\lambda^{BV} * (B-V) - \mu \tag{6}$$

Differentiating above equations.

$$\delta M_\lambda^0 = \delta m_\lambda - \delta R_\lambda^{BV} * E(B-V) - R_\lambda^{BV} * \delta E(B-V) - \delta\mu$$

$$\delta W_\lambda^{BV} = \delta m_\lambda - \delta R_\lambda^{BV} * (B-V) - R_\lambda^{BV} * \delta(B-V) - \delta\mu$$

Assume that the apparent luminosities are measured precisely ($\delta m_\lambda \to 0$) and that the adjusted extinction law is accurate ($\delta R \to 0$). Even so, the distance modulus ($\delta\mu$) and the color excess (δE_{BV}) may still contain errors for individual Cepheids. Under these conditions,

it follows that:

$$\delta M_\lambda = -(R_\lambda^{BV} * \delta E(B-V) + \delta\mu) \tag{7}$$

$$\delta W_\lambda^{BV} = -\delta\mu \tag{8}$$

This pair of equations indicates that both the Wesenheit magnitude and the absolute magnitude are sensitive to errors in distance. However, unlike the absolute magnitude, the Wesenheit magnitude is insensitive to errors in reddening. This key property of the Wesenheit magnitude is particularly useful for decoupling the error budget between distance and reddening when applied to Cepheids.

2. Galactic Cepheids: Leavitt Law

Classical Cepheids exhibit a linear relationship between their pulsation period ($\log P$) and their true luminosity (M_λ^0), which can be modeled as:

$$\bar{M}_\lambda = \alpha_\lambda(logP) + \gamma_\lambda \tag{9}$$

The dataset includes $BVIJHK$ photometry of Galactic Cepheids, resulting in six Leavitt Laws, each modeled by two parameters: the slope (α_λ) and the intercept (γ_λ).

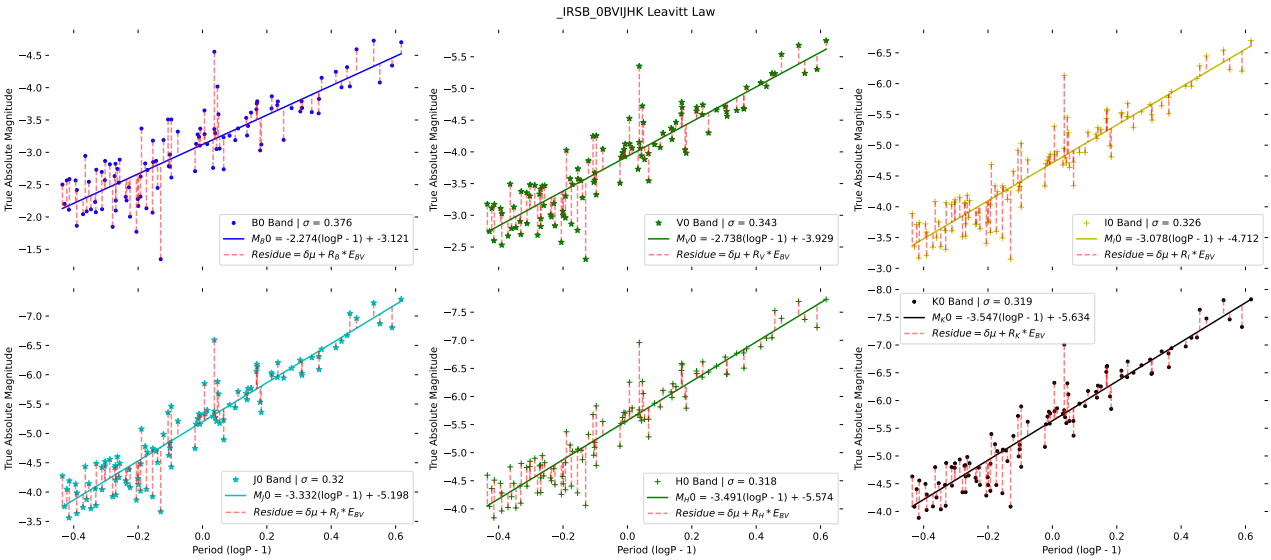

Figure 3: 109 Galactic Cepheids based BVIJHK Leavitt Law prior to calibration.

The deviation of the observed luminosity (M_λ^0) from the modeled value ($\bar{M}_\lambda$) is denoted as ΔM_λ.

$$\Delta M_\lambda = M_\lambda^0 - \bar{M}_\lambda$$

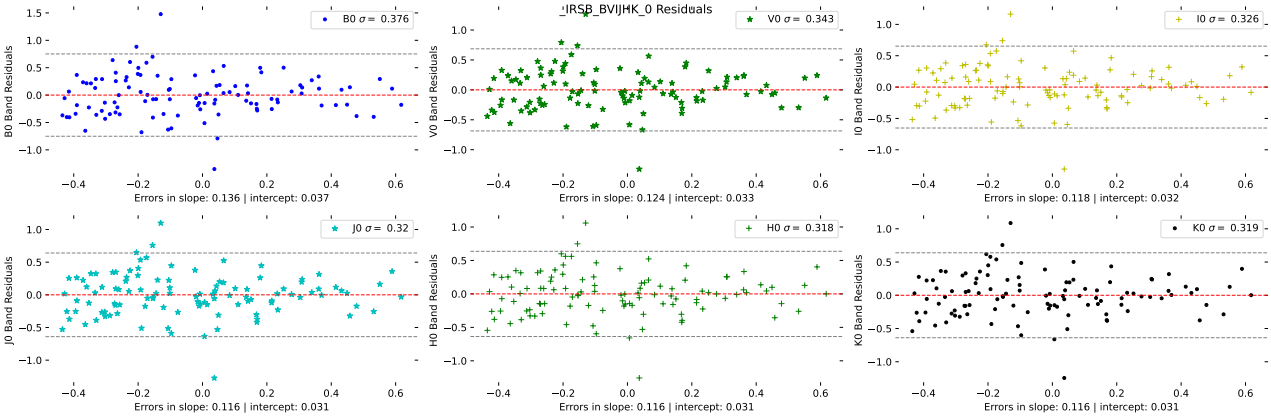

Figure 4: Residuals of the $BVIJHK$ Leavitt Laws show a decreasing scatter with increasing wavelength, indicating a dependence on interstellar extinction.

The Wesenheit magnitude - based Leavitt Law can be derived using a reference color index $(m_1 - m_2)$. For each combination of band and color index, the reddening-free form of the Leavitt Law can be modeled as:

$$\bar{W}_\lambda^{12} = \alpha_\lambda^{12}(logP) + \gamma_\lambda^{12} \tag{10}$$

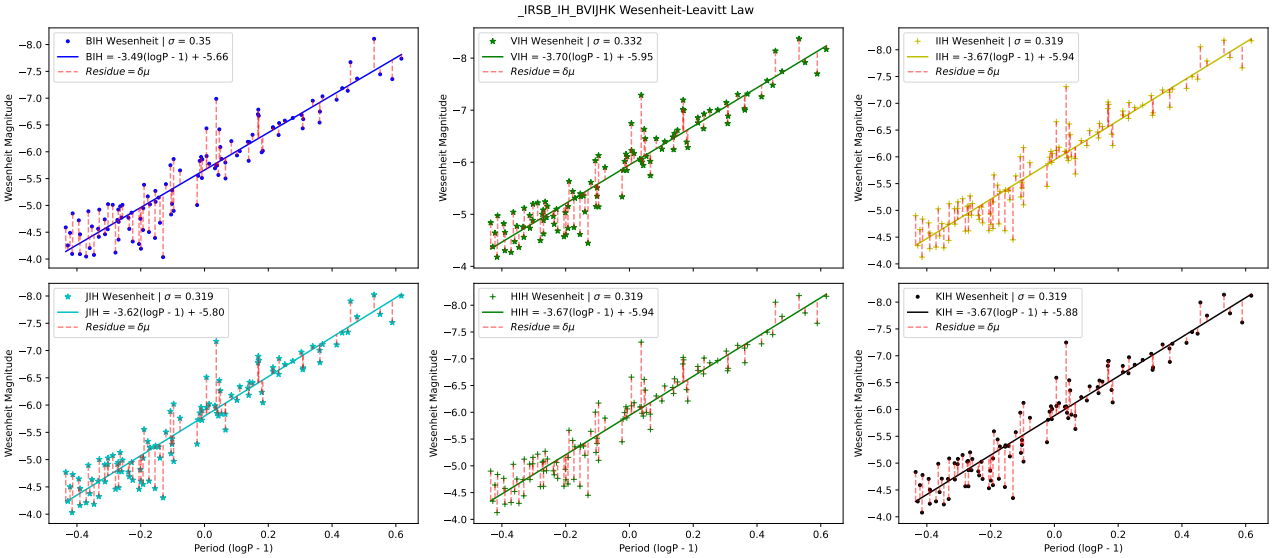

Figure 5: BVIJHK Period-Wesenheit Relation with respect to infrared color (I-H) for 109 Cepheids.

For $BVIJHK$ photometry, there are 15 possible combinations of color indices. Considering six observed bands with each color index results in 90 composite Wesenheit magnitudes (W_λ^{12}).

The deviation of the Wesenheit magnitude from the corresponding Period-Wesenheit (PW) relation is given by:

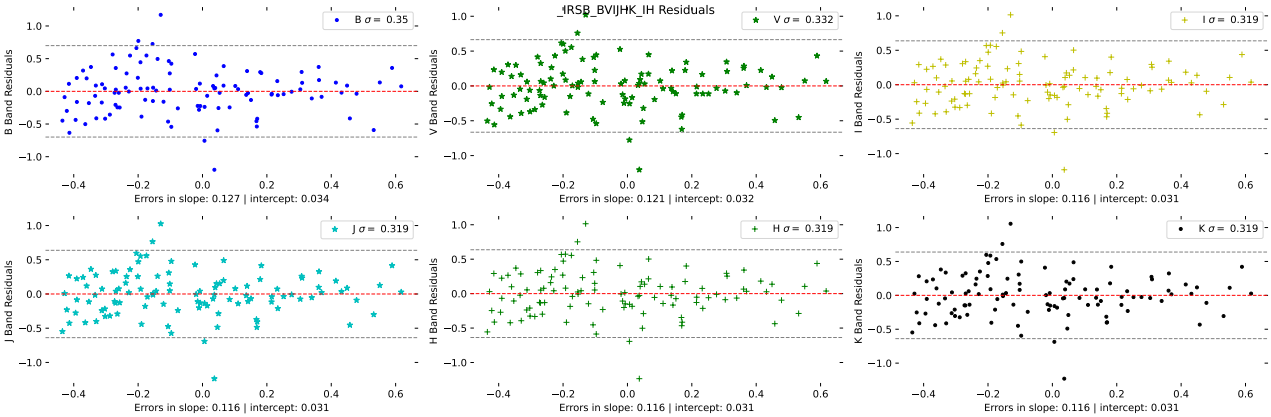

Figure 6: Residuals of the $BVIJHK$ Wesenheit-Leavitt Law for the $(I - H)$ color show an approximately constant scatter across all bands, upto 1 mag, indicating insensitivity to interstellar extinction. Given infrared bands, scatter is attributed primarily to distance modulus error.

$$\Delta W_\lambda^{12} = W_\lambda^{12} - \bar{W}_\lambda^{12}$$

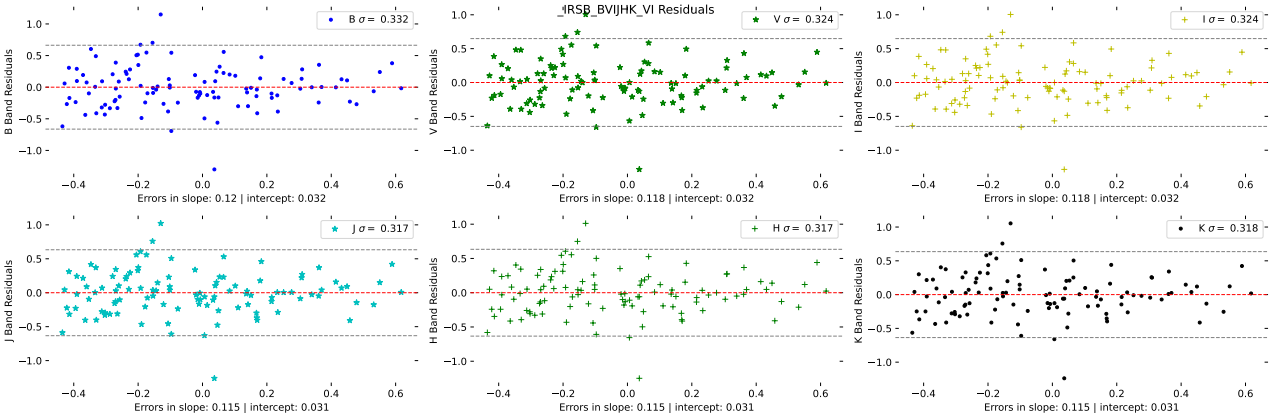

Figure 7: Residuals from the (V-I)-based Wesenheit Leavitt Law. Scatter remains constant, but distance errors are reduced compared to (I-H), compensating for reddening uncertainties.

Correlation between pulsation period and luminosity (true absolute and wesenheit) of Cepheids produces $6 + 90$ linear equations, each characterized by a slope and intercept, along with the residuals for each Cepheid. A summary is provided below in Table 1

$$\text{PL relation: } \alpha_\lambda \mid \gamma_\lambda \mid \Delta M_\lambda \mid \implies 6 \text{ equations}$$
$$\text{PW relation: } \alpha_\lambda^{12} \mid \gamma_\lambda^{12} \mid \Delta W_\lambda^{12} \implies 90 \text{ equations}$$

Table 2: Slope and Intercept of BVIJHK Leavitt Law using 109Galactic Cepheids

	B (err)	V (err)	I (err)	J (err)	H (err)	K (err)
Slope and Intercept of Period-Luminosity Relation						
Slope	-1.83 (0.159)	-2.26 (0.131)	-2.57 (0.105)	-2.79 (0.091)	-2.92 (0.086)	-2.97 (0.086)
Intercept	-4.45 (0.048)	-5.00 (0.039)	-5.37 (0.031)	-5.53 (0.027)	-5.79 (0.026)	-5.79 (0.026)
Slope of Period-Wesenheit Relations						
BV	-3.92 (0.132)	-3.92 (0.132)	-3.57 (0.113)	-3.28 (0.095)	-3.22 (0.089)	-3.18 (0.087)
BI	-3.25 (0.101)	-3.39 (0.105)	-3.25 (0.100)	-3.12 (0.091)	-3.12 (0.087)	-3.11 (0.086)
BJ	-3.08 (0.089)	-3.25 (0.094)	-3.17 (0.094)	-3.08 (0.089)	-3.10 (0.086)	-3.10 (0.085)
BH	-3.10 (0.085)	-3.27 (0.091)	-3.18 (0.092)	-3.09 (0.088)	-3.10 (0.085)	-3.10 (0.085)
BK	-3.10 (0.085)	-3.27 (0.090)	-3.18 (0.091)	-3.09 (0.088)	-3.10 (0.085)	-3.10 (0.085)
VI	-2.82 (0.097)	-3.04 (0.097)	-3.04 (0.097)	-3.02 (0.090)	-3.06 (0.086)	-3.07 (0.085)
VJ	-2.78 (0.088)	-3.01 (0.088)	-3.02 (0.090)	-3.01 (0.088)	-3.05 (0.085)	-3.07 (0.085)
VH	-2.84 (0.083)	-3.06 (0.084)	-3.05 (0.088)	-3.03 (0.087)	-3.06 (0.084)	-3.07 (0.084)
VK	-2.86 (0.084)	-3.07 (0.084)	-3.06 (0.088)	-3.03 (0.087)	-3.07 (0.084)	-3.07 (0.084)
IJ	-2.72 (0.102)	-2.97 (0.094)	-3.00 (0.088)	-3.00 (0.088)	-3.05 (0.085)	-3.06 (0.085)
IH	-2.87 (0.089)	-3.09 (0.085)	-3.07 (0.083)	-3.03 (0.086)	-3.07 (0.083)	-3.08 (0.084)
IK	-2.89 (0.090)	-3.10 (0.085)	-3.08 (0.084)	-3.04 (0.086)	-3.07 (0.083)	-3.08 (0.084)
JH	-3.27 (0.081)	-3.40 (0.079)	-3.26 (0.079)	-3.13 (0.081)	-3.13 (0.081)	-3.11 (0.082)
JK	-3.19 (0.088)	-3.34 (0.082)	-3.22 (0.081)	-3.11 (0.083)	-3.11 (0.082)	-3.11 (0.083)
HK	-3.04 (0.159)	-3.22 (0.131)	-3.15 (0.105)	-3.07 (0.091)	-3.09 (0.086)	-3.09 (0.086)
Intercept of Period-Wesenheit Relations						
BV	-7.11 (0.039)	-7.11 (0.039)	-6.66 (0.034)	-6.16 (0.029)	-6.17 (0.027)	-6.05 (0.026)
BI	-6.24 (0.030)	-6.42 (0.031)	-6.24 (0.030)	-5.96 (0.027)	-6.05 (0.026)	-5.96 (0.026)
BJ	-5.87 (0.027)	-6.12 (0.028)	-6.06 (0.028)	-5.87 (0.027)	-5.99 (0.026)	-5.93 (0.025)
BH	-6.02 (0.025)	-6.24 (0.027)	-6.13 (0.027)	-5.90 (0.026)	-6.02 (0.025)	-5.94 (0.025)
BK	-5.94 (0.025)	-6.18 (0.027)	-6.09 (0.027)	-5.89 (0.026)	-6.00 (0.025)	-5.94 (0.025)
VI	-5.66 (0.029)	-5.96 (0.029)	-5.96 (0.029)	-5.82 (0.027)	-5.96 (0.026)	-5.91 (0.025)
VJ	-5.42 (0.026)	-5.76 (0.026)	-5.84 (0.027)	-5.76 (0.026)	-5.93 (0.025)	-5.88 (0.025)
VH	-5.67 (0.025)	-5.96 (0.025)	-5.96 (0.026)	-5.82 (0.026)	-5.96 (0.025)	-5.91 (0.025)
VK	-5.59 (0.025)	-5.90 (0.025)	-5.93 (0.026)	-5.80 (0.026)	-5.95 (0.025)	-5.90 (0.025)
IJ	-5.10 (0.031)	-5.51 (0.028)	-5.69 (0.026)	-5.69 (0.026)	-5.88 (0.025)	-5.85 (0.025)
IH	-5.68 (0.027)	-5.97 (0.025)	-5.97 (0.025)	-5.82 (0.026)	-5.97 (0.025)	-5.91 (0.025)
IK	-5.53 (0.027)	-5.85 (0.025)	-5.89 (0.025)	-5.79 (0.026)	-5.94 (0.025)	-5.89 (0.025)
JH	-7.23 (0.024)	-7.21 (0.024)	-6.72 (0.024)	-6.19 (0.024)	-6.19 (0.024)	-6.06 (0.024)
JK	-6.29 (0.026)	-6.46 (0.024)	-6.27 (0.024)	-5.97 (0.025)	-6.05 (0.024)	-5.97 (0.025)
HK	-4.45 (0.048)	-5.00 (0.039)	-5.37 (0.031)	-5.53 (0.027)	-5.79 (0.026)	-5.79 (0.026)

2.1 PL-PW Residuals

A crucial difference between the two types of relations is that the residuals of the Period-Wesenheit (PW) relation are assumed to be free from reddening errors, whereas those of the Period-Luminosity (PL) relation are not. The correlation between the PL and PW residuals ($\Delta M - \Delta W$ correlation) provides quantitative insights into the error budget associated with reddening and distance modulus. To develop a mathematical framework, two cases must be considered:

i) When there is error only in distance, ($\delta\mu \neq 0$, $\delta E_{12} = 0$):

$$\text{Deviation in PL} : \Delta M_\lambda = \delta\mu$$
$$\text{Deviation in PW} : \Delta W_\lambda^{12} = \delta\mu$$

In the residual correlation plots, *an error in distance shifts the star equally along both axes from its original position*, meaning that Cepheid with minimal or no reddening error would lie perfectly along a line with slope 1. This behavior is clearly evident in the infrared bands, where reddening errors are expected to be minimal at longer wavelengths.

ii) When there is error in reddening alone, ($\delta E_{12} \neq 0$, $\delta\mu = 0$):

$$\text{Deviation in PL} : \Delta M_\lambda = R^{12}_\lambda \delta E_{12}$$
$$\text{Deviation in PW} : \Delta W^{12}_\kappa = 0$$

In this case, only the PL residuals are affected, whereas the PW residuals remain unchanged, since the Wesenheit magnitude is reddening - independent by definition. This means that the star shifts along the PL residual axis but not along the PW residual axis. Consequently, *a vertical displacement of the star in Δ–Δ plots originates from the reddening error.*

3. Distance - Reddening Calibration Methodology

To decouple the reddening and distance errors for individual Cepheids, the residuals of the PL relations (ΔM_λ) are plotted against the corresponding PW residuals (ΔW^{12}_κ). Fitting a regression line with slope $\rho^{12}_{\kappa\lambda}$ and zero intercept yields the residuals for each band and choice of Wesenheit color. The resulting $\Delta - \Delta$ residuals are denoted as:

$$\Delta^{12}_{\kappa\lambda} = \Delta M_\lambda - \rho^{12}_{\kappa\lambda} \times \Delta W^{12}_\kappa$$

This vertical deviation from the regression line indicates the extinction correction for the corresponding band, without considering any correction to the distance modulus.

$$\delta A^{12}_{\kappa\lambda}(0) = \Delta^{12}_{\kappa\lambda}$$

By normalizing with R^{12}_λ, the extinction corrections ($\delta A^{12}_{\kappa\lambda}$) are converted into reddening corrections ($\delta E^{12}_{\kappa\lambda}$) as follows:

$$\delta E^{12}_{\kappa\lambda}(0) = \frac{\delta A^{12}_{\kappa\lambda}}{R^{12}_\lambda}$$

If the distances of individual targets are precisely known, then reddening is the sole source of error. This implies that the corrections indicated by each band should be consistent with one another.

$$\delta E^{12}_{\kappa B} = \delta E^{12}_{\kappa V} = ... = \delta E^{12}_{\kappa K} = \delta E^{*}_{12}$$

If distances are accurately known, the reddening corrections derived from different bands would show no dispersion, as discussed above. In contrast, an incorrect distance for a given Cepheid would result in discrepancies among the reddening corrections estimated from the various bands.

To estimate the distance error, a range of possible distance corrections ($\delta\mu^i$) is considered. For each assumed correction, the reddening corrections for all bands are computed. The particular distance correction for which the reddening corrections are most consistent across all bands (i.e., exhibiting minimal variation) is adopted as the optimal distance – reddening correction pair for the individual Cepheid.

The variation in extinction ($\delta A^{12}_{\kappa\lambda}$) resulting from a distance modulus correction is calculated as follows:

$$\begin{aligned}\delta A^{12}_{\kappa\lambda}(\delta\mu) &= (\Delta M_\lambda + \delta\mu) - \rho^{12}_{\kappa\lambda} \times (\Delta W^{12}_{\kappa} + \delta\mu) \\ &= \delta A^{12}_{\kappa\lambda}(0) + \delta\mu(1 - \rho^{12}_{\kappa\lambda})\end{aligned}$$

The corresponding reddening corrections are then given by:

$$\delta E^{12}_{\kappa\lambda}(\delta\mu) = \delta E^{12}_{\kappa\lambda}(0) + \frac{\delta\mu(1 - \rho^{12}_{\kappa\lambda})}{R^{12}_{\lambda}} \tag{11}$$

For the optimal distance - reddening correction pair, the dispersion in the estimated reddening corrections from the BVIJHK bands is minimized.

$$RMS(\delta E(\delta\mu))_\lambda = \frac{1}{6}\sum_{\lambda}(\delta E^{12}_{\kappa\lambda}(\delta\mu) - < \delta E^{12}_{\kappa\lambda}(\delta\mu) >_\lambda)^2$$

$$min(RMS(\delta E(\delta\mu))_\lambda)_\mu \implies (\delta\mu^*, \delta E^*_{12})$$

These corrections are then applied to the original data as follows:

$$M^*_\lambda = M^0_\lambda + \delta A^*_\lambda + \delta\mu^* \tag{12}$$

3.1 Madore Approach

In his analysis, Madore et al. (2017) used W^{VI}_V as the reference reddening-free magnitude.. He correlated the PW residuals (ΔW^{VI}_V) with BVRIJHK PL residuals (ΔM_λ) to derive the corresponding slopes ($\rho^{VI}_{V\lambda}$) and residuals ($\Delta^{VI}_{V\lambda}$). Here, I will demonstrate the difference between his approach and mine for calibrating the Leavitt Law.

Let $\delta\mu^*$ denote the correction required in the distance modulus. Then, the reddening cor-

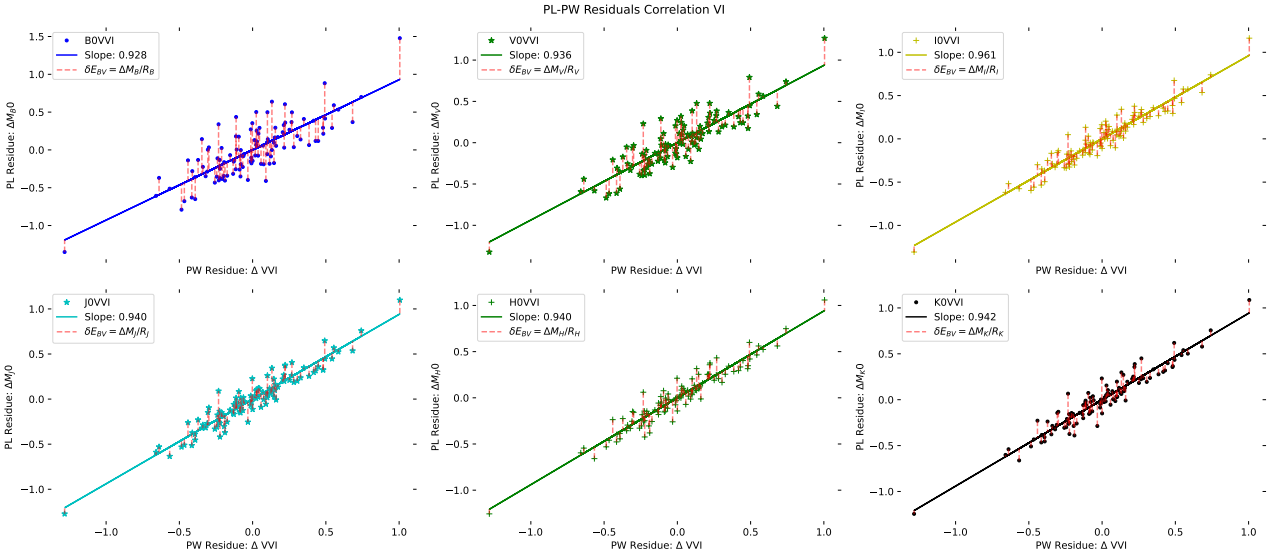

(a) Residual correlation according to Madore (2017), where the y-axis represents the residuals of the PL relation (ΔM_λ) and the x-axis, fixed for all six bands, represents the residuals of the PW relation (ΔW_V^{VI}).

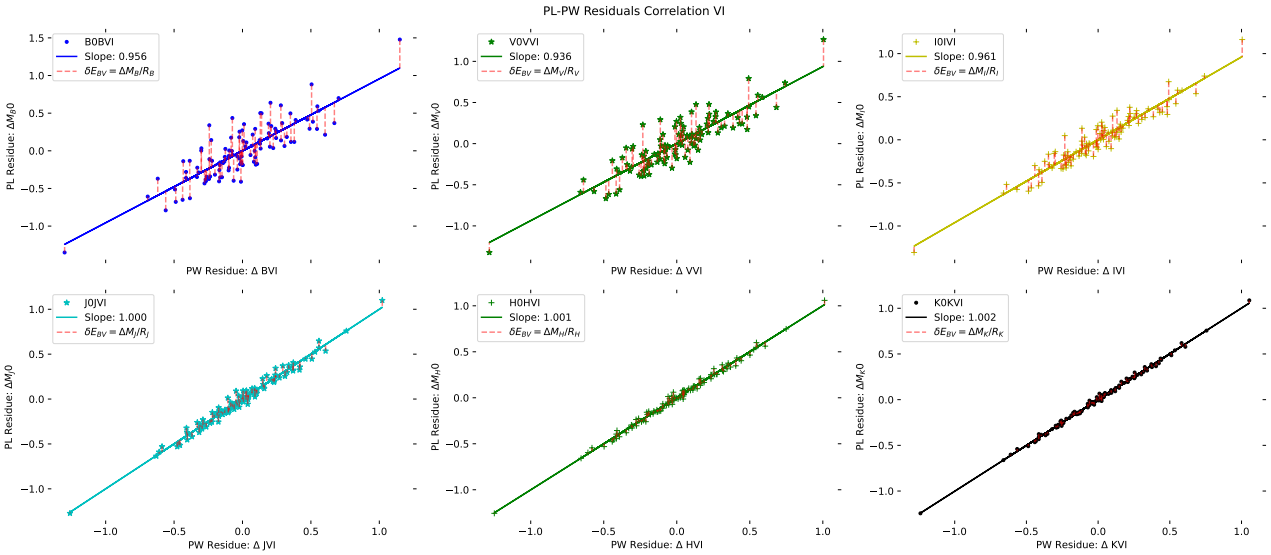

(b) Different than Madore's approach, here for each band of PL residual (ΔM_λ), respective reddening free residual (ΔW_λ^{VI}) plotted along x axis.

Figure 8: Comparison of the slopes - bottom panel approaches 1 more rapidly with increasing wavelength decoupling modulus error effectively.

rections $\delta E^{VI}_{V\lambda}$, as derived by Madore (2017), are given by:

$$\delta E^{VI}_{V\lambda}(\delta\mu^*) = \frac{\delta A^{VI}_{V\lambda}(\delta\mu^*)}{R^{VI}_{\lambda}}$$

Converting E_{VI} into E_{BV}

$$\begin{aligned}\delta E^{BV}_{V\lambda}(\delta\mu^*) &= \frac{\delta A^{VI}_{V\lambda}(\delta\mu^*)}{(R^{BV}_{V} - R^{BV}_{I})R^{VI}_{\lambda}} \\ &= \frac{\delta A^{VI}_{V\lambda}(\delta\mu^*)}{R^{BV}_{\lambda}}\end{aligned}$$

By implementing these reddening and distance error corrections in his dataset of 59 Cepheids, he derived the Leavitt Laws as given in Table 3:

Table 3: Madore (2017): Slope and Intercept of Galactic BVIJHK Leavitt Law

Band	Slope	σ (mag)	Zero	σ (mag)
B	-2.277	0.121	-3.214	0.036
V	-2.670	0.095	-3.944	0.028
R	-2.874	0.075	-4.396	0.022
I	-2.983	0.064	-4.706	0.019
J	-3.198	0.054	-5.258	0.016
H	-3.333	0.055	-5.558	0.017
K	-3.377	0.055	-5.659	0.016
W(VI)	-3.476	0.037	-5.889	0.011
W(BI)	-3.600	0.033	-5.997	0.010

3.2 My Approach

Instead of keeping ΔW^{VI}_{V} fixed, I have used ΔW^{VI}_{λ} — the reddening free magnitude for the respective band. This choice follows directly from the definition of the Wesenheit function: the reddening - free magnitude for a given band must be derived using R^{12}_{λ}, not R^{12}_{V}. Specifically, R^{VI}_{V} gives the wesenheit magnitude corresponding to the V band only for the $(V-I)$ color index. For the B band, $R^{VI}_{B}(V-I)$ must be subtracted from B to obtain the corresponding Wesenheit magnitude. Consequently, the PW residuals along x-axis in my approach will be varying with the respective PL residuals ΔM_{λ}. The difference between Madore's and my PW residuals is represented by the operator δ^{λ}_{V} and is calculated as follows:

$$
\begin{aligned}
\delta_V^{\lambda}\Delta W_{\lambda}^{VI} &= \Delta W_{\lambda}^{VI} - \Delta W_{V}^{VI} \\
&= (W_{\lambda}^{VI} - \bar{W}_{\lambda}^{VI}) - (W_{V}^{VI} - \bar{W}_{V}^{VI}) \\
&= (W_{\lambda}^{VI} - W_{V}^{VI}) - (\bar{W}_{\lambda}^{VI} - \bar{W}_{V}^{VI}) \\
&= ((M_{\lambda} - M_{V}) - (R_{\lambda}^{VI} - R_{V}^{VI})(V - I)) - ((\alpha_{\lambda}^{VI} - \alpha_{V}^{VI}) \log P + (\gamma_{\lambda}^{VI} - \gamma_{V}^{VI}))
\end{aligned}
$$

This deviation in the PW residuals affects the slope of the regression line, ρ, which implies that the correlation residuals, $\Delta_{\kappa\lambda}^{12}$, will also be affected. In Madore's approach, the $\Delta - \Delta$ correlation residuals are expressed as $\Delta_{V\lambda}^{VI}$, since he correlated ΔM_{λ} with ΔW_{V}^{VI}. In contrast, I have correlated ΔM_{λ} with ΔW_{λ}^{VI}, so that the resulting residuals take the form $\Delta_{\lambda\lambda}^{VI}$.

Difference between both kinds of correlation residuals is:

$$
\begin{aligned}
\delta_{V\lambda}^{\lambda\lambda}\Delta_{\lambda\lambda}^{VI} &= \Delta_{\lambda\lambda}^{VI} - \Delta_{V\lambda}^{VI} \\
&= \delta A_{\lambda}^{S}(0) - A_{\lambda}^{M}(0) \\
&= (\Delta M_{\lambda} - \rho_{\lambda\lambda}^{VI} \times \Delta W_{\lambda}^{VI}) - (\Delta M_{\lambda} - \rho_{V\lambda}^{VI} \times \Delta W_{V}^{VI}) \\
&= \rho_{V\lambda}^{VI} \times \Delta W_{V}^{VI} - \rho_{\lambda\lambda}^{VI} \times \Delta W_{\lambda}^{VI}
\end{aligned}
$$

3.3 Physical Significance of Residual-Slope

The slope of the PL–PW residual correlation quantifies the contributions of error sources. With no extinction errors, the distance remains the sole source of uncertainty, affecting both axes equally and resulting in a slope of 1.

$$
\lim_{\lambda \to \infty} \rho_{\lambda\lambda}^{12} = 1 \tag{13}
$$

This behavior is particularly evident at longer wavelengths, such as the K band shown in Table 4. The yellow-highlighted cases represent the slopes, ρ, obtained using my approach. This is not observed in Madore's approach, as it uses a fixed PW residual for all bands along the y-axis, resulting in deviation from slope 1. To illustrate this more clearly, consider the case of an incorrect reddening law, R_{λ}^{12}, where ΔW_{λ}^{12} takes the form:

$$
\Delta W_{\lambda}^{12} = -\delta\mu - \delta R_{\lambda}^{12}(m_1 - m_2)
$$

which affects ρ as follows:

Table 4: Variation of the $\Delta - \Delta$ correlation slope, $\rho^{12}_{\kappa\lambda}$, for fifteen Wesenheit colors, comparing Madore's approach (white) with my approach (yellow). The $(V - I)$ case is highlighted in red. The continuous decrease in slope-error with increasing wavelength, aligning along a slope of 1, is a strong indication of larger distance error with respect .

ρ	B (err)	V (err)	I (err)	J (err)	H (err)	K (err)
BV	0.243 (0.084)	0.398 (0.067)	0.471 (0.056)	0.479 (0.050)	0.478 (0.045)	0.471 (0.046)
	0.243 (0.084)	0.398 (0.067)	0.653 (0.054)	0.870 (0.035)	0.929 (0.024)	0.962 (0.017)
BI	0.652 (0.092)	0.758 (0.066)	0.831 (0.045)	0.798 (0.040)	0.773 (0.035)	0.765 (0.036)
	0.652 (0.092)	0.683 (0.068)	0.832 (0.045)	0.944 (0.025)	0.968 (0.016)	0.982 (0.011)
BJ	0.881 (0.090)	0.945 (0.060)	0.975 (0.041)	0.972 (0.021)	0.938 (0.014)	0.933 (0.016)
	0.881 (0.090)	0.835 (0.066)	0.920 (0.041)	0.972 (0.021)	0.981 (0.014)	0.990 (0.009)
BH	0.917 (0.096)	0.983 (0.065)	1.015 (0.045)	1.017 (0.025)	0.988 (0.014)	0.984 (0.014)
	0.917 (0.096)	0.859 (0.070)	0.941 (0.043)	0.983 (0.022)	0.988 (0.014)	0.995 (0.009)
BK	0.945 (0.094)	0.996 (0.064)	1.022 (0.045)	1.023 (0.024)	0.992 (0.014)	0.994 (0.009)
	0.945 (0.094)	0.880 (0.069)	0.951 (0.042)	0.986 (0.021)	0.990 (0.013)	0.994 (0.009)
VI	0.787 (0.086)	0.847 (0.060)	0.907 (0.037)	0.854 (0.035)	0.820 (0.032)	0.813 (0.034)
	0.870 (0.077)	0.847 (0.060)	0.907 (0.037)	0.974 (0.020)	0.984 (0.013)	0.991 (0.009)
VJ	0.938 (0.087)	0.980 (0.057)	1.000 (0.039)	0.994 (0.017)	0.956 (0.010)	0.953 (0.011)
	1.053 (0.072)	0.980 (0.057)	0.990 (0.034)	0.994 (0.017)	0.994 (0.011)	0.996 (0.007)
VH	0.951 (0.094)	1.004 (0.064)	1.031 (0.045)	1.031 (0.023)	1.001 (0.012)	0.998 (0.012)
	1.087 (0.082)	1.004 (0.064)	1.011 (0.037)	1.006 (0.018)	1.001 (0.012)	1.002 (0.008)
VK	0.965 (0.093)	1.007 (0.063)	1.030 (0.045)	1.030 (0.023)	0.998 (0.013)	1.001 (0.008)
	1.080 (0.080)	1.007 (0.063)	1.013 (0.037)	1.008 (0.018)	1.001 (0.011)	1.001 (0.008)
IJ	0.939 (0.087)	0.969 (0.060)	0.969 (0.047)	0.985 (0.023)	0.948 (0.017)	0.946 (0.017)
	0.764 (0.079)	0.814 (0.069)	0.969 (0.047)	0.985 (0.023)	0.992 (0.014)	0.996 (0.010)
IH	0.956 (0.096)	1.005 (0.066)	1.024 (0.049)	1.036 (0.026)	1.007 (0.015)	1.005 (0.014)
	0.856 (0.095)	0.891 (0.079)	1.024 (0.049)	1.013 (0.023)	1.007 (0.015)	1.007 (0.010)
IK	0.969 (0.093)	1.008 (0.064)	1.025 (0.048)	1.032 (0.025)	1.001 (0.015)	1.005 (0.010)
	0.868 (0.090)	0.906 (0.076)	1.025 (0.048)	1.013 (0.023)	1.007 (0.014)	1.005 (0.010)
JH	0.941 (0.104)	1.008 (0.073)	1.044 (0.054)	1.053 (0.034)	1.032 (0.021)	1.030 (0.020)
	0.477 (0.133)	0.654 (0.112)	0.977 (0.072)	1.053 (0.034)	1.032 (0.021)	1.027 (0.014)
JK	0.969 (0.096)	1.011 (0.067)	1.035 (0.049)	1.038 (0.029)	1.010 (0.018)	1.016 (0.012)
	0.678 (0.110)	0.788 (0.096)	1.000 (0.060)	1.038 (0.029)	1.024 (0.018)	1.016 (0.012)
HK	0.962 (0.090)	0.984 (0.063)	0.998 (0.048)	0.997 (0.030)	0.964 (0.024)	0.976 (0.016)
	0.375 (0.061)	0.445 (0.064)	0.703 (0.058)	0.911 (0.035)	0.964 (0.024)	0.976 (0.016)

Madore (for $(V - I)$):

$$\rho^{VI}_{V\lambda} = \frac{-\delta\mu - \delta A_\lambda}{-\delta\mu - \delta R^{VI}_V (V - I)} \tag{14}$$

As the wavelength increases, δA_λ decreases, while δR^{VI}_V remains fixed, causing the resulting ratio to be smaller than 1 even at longer wavelengths.

Shubham (for $(V - I)$):

$$\rho^{VI}_{\lambda\lambda} = \frac{-\delta\mu - \delta A_\lambda}{-\delta\mu - \delta R^{VI}_\lambda (V - I)} \tag{15}$$

Here, both δA_λ and δR^{VI}_λ decrease with increasing wavelength, causing the numerator and denominator to converge, and the slope approaches 1 at longer wavelengths.

Since the deviation between $\rho_{V\lambda}^{VI}$ and $\rho_{\lambda\lambda}^{VI}$ is non-zero, the derived reddening corrections will also differ from those of Madore. The difference between the two reddening errors, prior to distance correction, can be expressed as:

$$\begin{aligned}\delta E_{\lambda\lambda}^{VI}(0) - \delta E_{V\lambda}^{VI}(0) &= \frac{\delta A_{\lambda\lambda}^{VI}(0) - \delta A_{V\lambda}^{VI}(0)}{R_{\lambda}^{VI}} \\ &= \frac{\Delta_{\lambda\lambda}^{VI} - \Delta_{V\lambda}^{VI}}{R_{\lambda}^{VI}} \\ &= \frac{\Delta W_{\lambda}^{VI} \times \rho_{\lambda\lambda}^{VI} - \Delta W_{V}^{VI} \times \rho_{V\lambda}^{VI}}{R_{\lambda}^{VI}}\end{aligned}$$

Determination of distance correction ($\delta\mu^*$) requires scaling factor ($1-\rho_{\kappa\lambda}^{12}$), implies distance correction would also be different.

4. Tweaking Distance - Reddening Calibration Method

Given multiple photometric bands, shorter wavelengths are more sensitive to reddening uncertainties, while distance errors are largely wavelength-independent. To mitigate this, distance and reddening are estimated in two stages. First, the longer-wavelength $IJHK$ bands provide an initial distance - reddening correction via an infrared $(I-H)$ Wesenheit color, offering robust distance estimates with minimal reddening adjustment. These corrected values are then refined using the shorter-wavelength $BVIJ$ bands and the $(V-J)$ Wesenheit index, which improves reddening accuracy with little effect on corrected distance. The final corrections produce a tightly constrained Galactic Leavitt Law across the $BVIJHK$ bands, with dispersions of 0.087 mag in B and 0.011 mag in K. The next section details the calibration procedure.

4.1 Distance correction using IJHK photometry

To derive the distance correction, I used the longer-wavelength $IJHK$ bands, which are weakly affected by extinction, excluding the more sensitive B and V bands to avoid bias from optical reddening. The correction was estimated using Wesenheit indices based on $(I-J)$, $(I-H)$, $(I-K)$, and $(J-K)$ colors, yielding a converging distance correction estimate with minimal reddening contamination.

For the colors $(I-J)$, $(I-H)$, $(I-K)$, and $(J-K)$, the Wesenheit magnitudes remain effectively reddening - free even in the presence of intrinsic uncertainties in the extinction law, as described by Equation 15. This is supported by the highly consistent values of $\delta\mu$ across all four colors (see Fig. 10). To illustrate the decoupling of distance and reddening errors, residual-correlation plots for the $(J-K)$ and $(I-H)$ colors are shown (see Fig. 9).

After applying the first-order distance-reddening corrections to individual Cepheids using the (I-H)-based Wesenheit, updated Leavitt Laws are derived, as shown in Fig. 11. To achieve

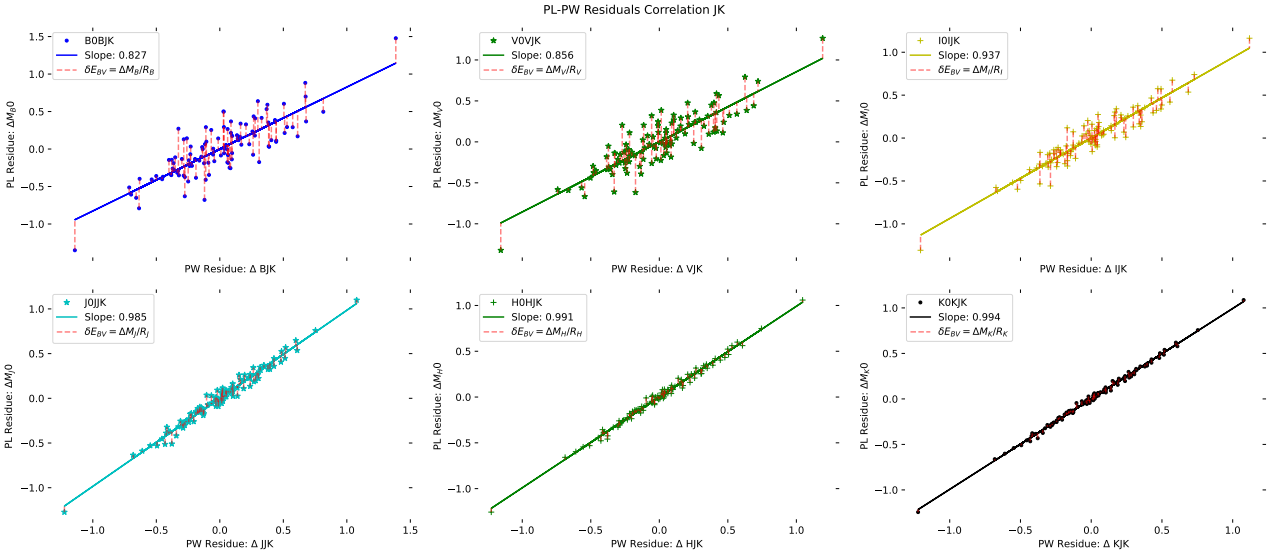

(a) ΔM_λ - ΔW_λ^{JK} correlation. Notice the relative scatter in between BV and $IJHK$ bands.

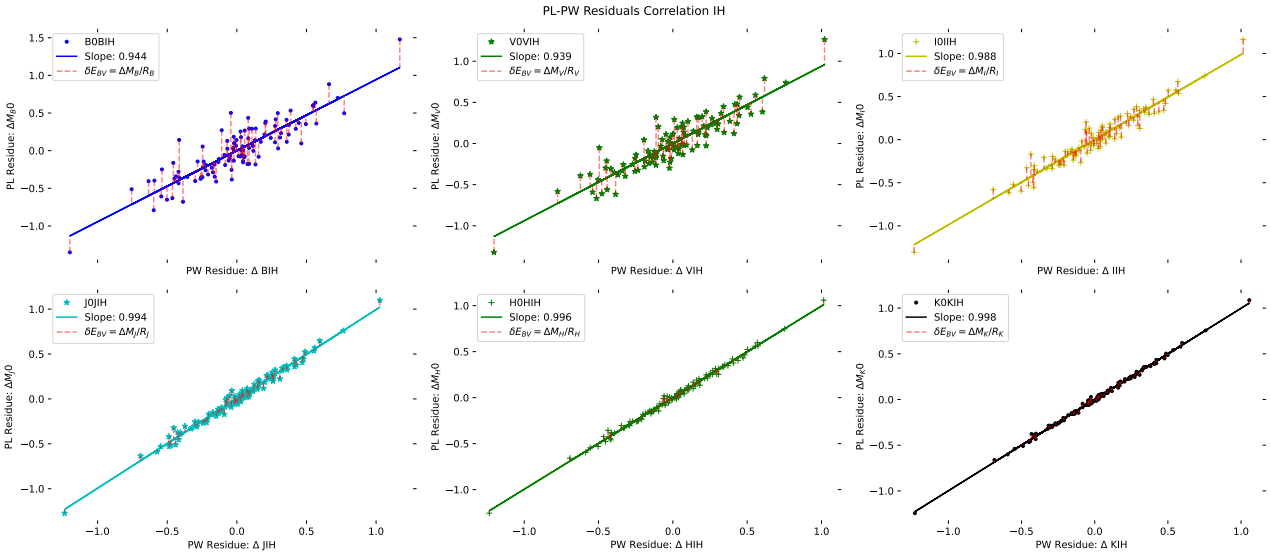

(b) Rapid inclination to 1 for ΔM_λ - ΔW_λ^{IH} correlation suggesting lesser sensitivity for reddening, better case for decopling distance error.

Figure 9: In the case of (I-H), the slope is closely aligned with 1, indicating weak sensitivity to reddening errors, making it a better standard for estimating distance errors.

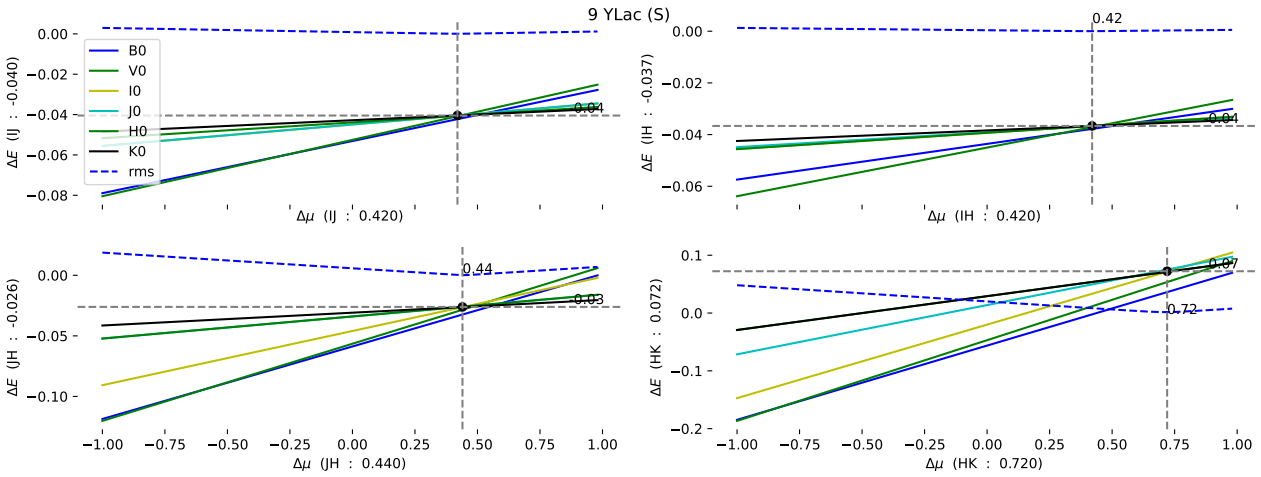

(a) Y Lac

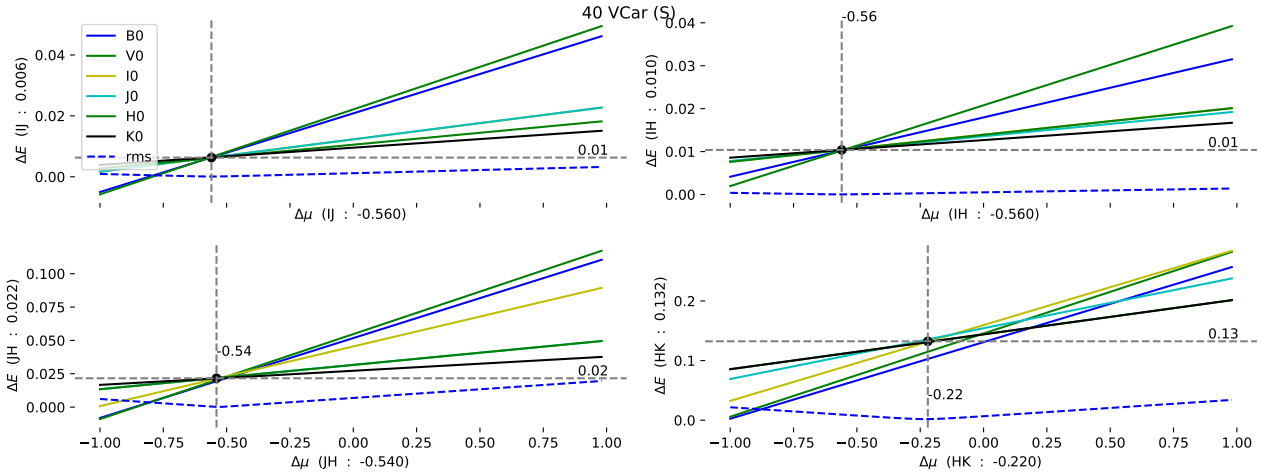

(b) V Car

Figure 10: $(I-J)$, $(I-H)$, $(J-H)$, and $(H-K)$ based modulus correction. The least dispersion among I, J, H, and K bands gives the correction pair $(\delta\mu, \delta E)$. The B and V bands are excluded. Each of the case suggest first order modulus correction for its respective color.

even higher accuracy, a second-order modulus-reddening correction for the (I-H)-calibrated data is derived in the next section.

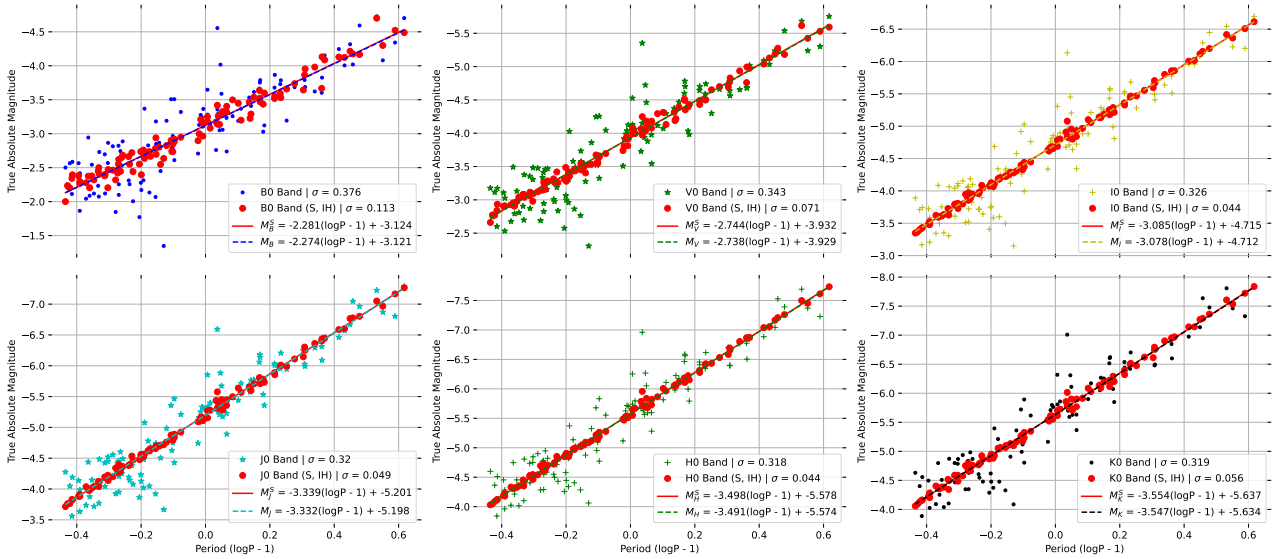

Figure 11: Distance calibration using the $(I-H)$–based Wesenheit index, with the B and V bands excluded, yields minimal reddening effects and high accuracy in distance estimates. The resulting distance correction is then applied uniformly across all bands. | Colored: Original Data | Red : Corrected Data

4.2 Reddening correction using BVIJ photometry

To obtain an accurate reddening correction, the optical and near - infrared bands ($BVIJ$) are used, while the H and K bands are excluded when estimating minimum variance accross the bands for reddening estimation. Using the first - order distance – reddening corrected data, the PL – PW residual correlation is re - evaluated. Since the remaining distance correction is expected to be minimal, the residual slope in this second - order correction should not approach unity as rapidly as observed in the first-order case. This can be clearly seen in Fig. 12

The high dispersion in the residual – slopes for the second-order correction clearly demonstrates the effectiveness of the first-order distance correction, as the systematic trend with a slope of unity is no longer followed with increasing wavelength. It is also noteworthy that the range of PL residuals (y - axis) decreases rapidly across the bands, indicating significant contamination from extinction errors still present. The reddening uncertainty can thus be quantified by identifying the distance solution that minimizes dispersion across the bands. Given the first order correction, further distance correction must be near-zero value.

The robustness of this approach is illustrated for two stars, as shown in Figure 13. For the given sample of Cepheids, the reddening errors derived from different colors show strong mutual agreement, requiring little to no additional distance correction across all bands. For individual Cepheids, applying these optical-based corrections yields the final calibrated results.

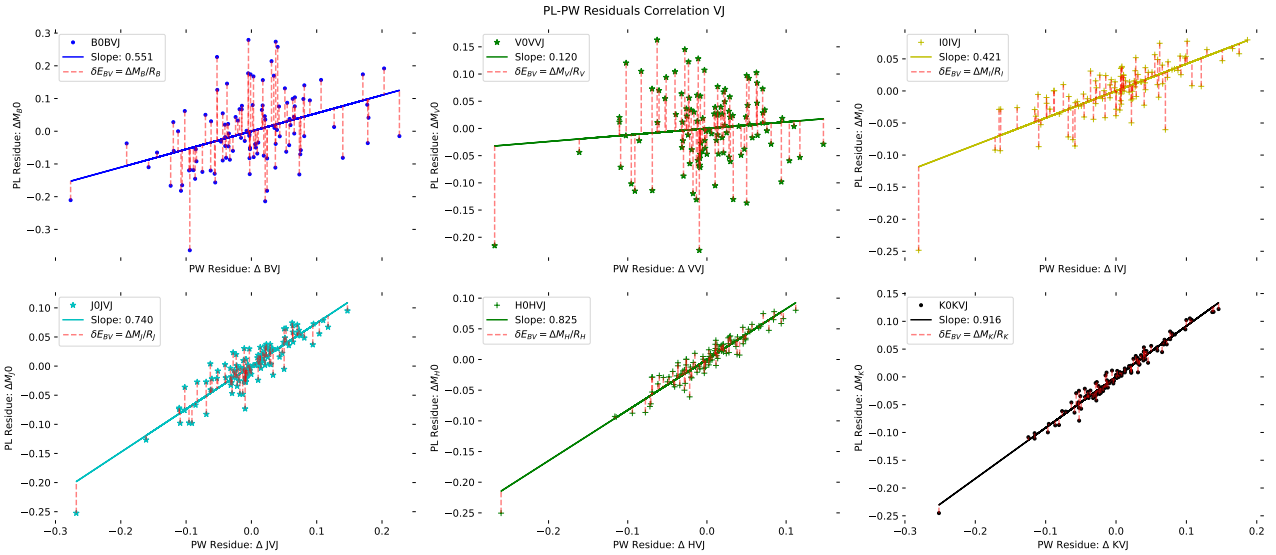

Figure 12: (V-J) based residual correlation for (I-H) based modulus-reddening calibrated data (first order correction). High variation in slope indicating absence of systematic effect of distance error, depicting bandwise extinction or reddening ratio related error contribution.

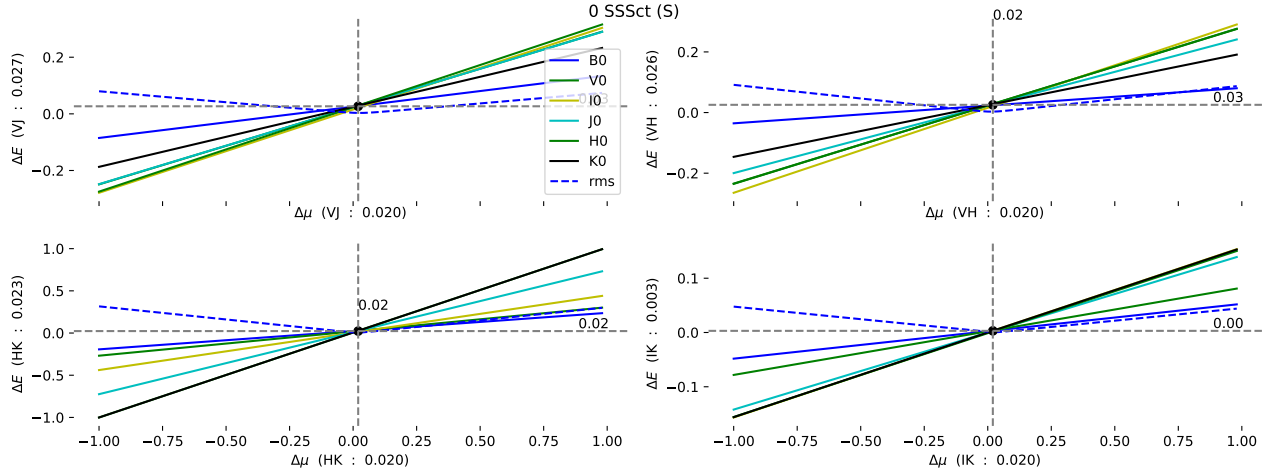

(a) SS Sct

Figure 13: $(V-J)$, $(V-H)$, $(H-K)$, and $(I-K)$ based reddening correction. Notice the consistency in reddening and modulus correction accross the colors in these instances of second order correction. Not all of the are correct but suggest systematics errors, possibly from photometric measures, extinction law and reddening ratio towards the line of sight of individual Cepheid.

5. Calibrated Leavitt Law

Each Cepheid in the dataset is corrected for distance and reddening, yielding calibrated true absolute magnitudes in the $BVIJHK$ bands. This produces a calibrated Leavitt Law, for which the $(I-H)$–based modulus and $(V-J)$–based reddening exhibit the least scatter for the set of 109 Cepheids.

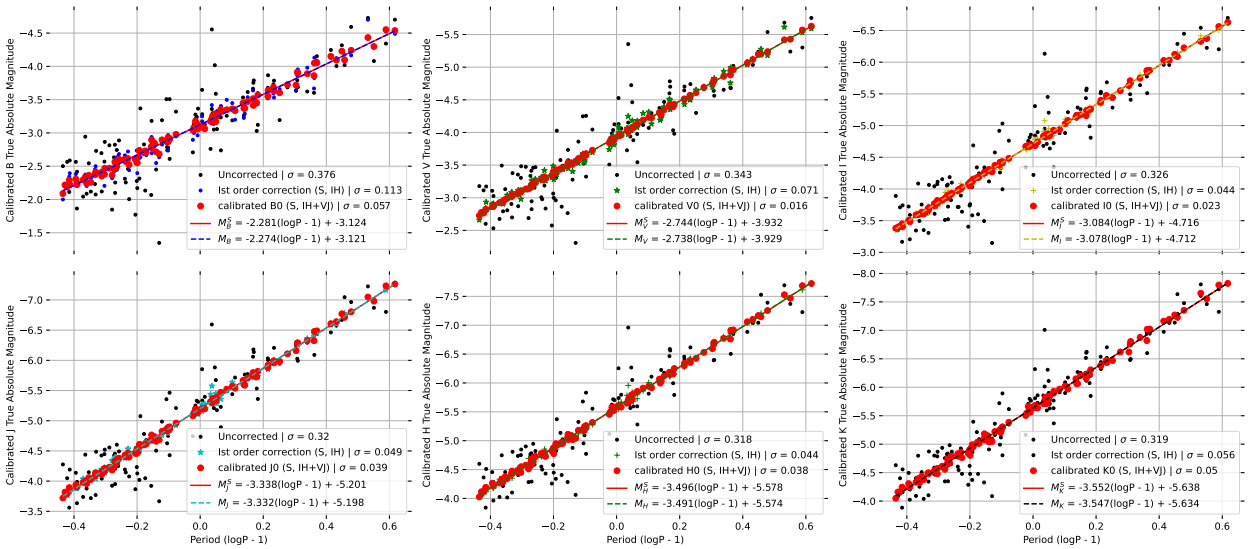

Figure 14: (V-J) based reddening correction (second - order) consistent with (I-H) color based first order correction.

109-Cepheids-IRSB-based calibrated Galactic Leavitt Law are:

$$
\begin{aligned}
M_B\,(0.057) &= (-2.281 \pm 0.021)(\log P - 1) - 3.124 \pm 0.006 \\
M_V\,(0.016) &= (-2.744 \pm 0.006)(\log P - 1) - 3.932 \pm 0.002 \\
M_I\,(0.023) &= (-3.084 \pm 0.008)(\log P - 1) - 4.716 \pm 0.002 \\
M_J\,(0.039) &= (-3.338 \pm 0.014)(\log P - 1) - 5.201 \pm 0.004 \\
M_H\,(0.038) &= (-3.496 \pm 0.014)(\log P - 1) - 5.578 \pm 0.004 \\
M_K\,(0.050) &= (-3.552 \pm 0.018)(\log P - 1) - 5.638 \pm 0.005
\end{aligned}
$$

$$
\begin{aligned}
W_B^{BI}\,(0.055) &= (-3.839 \pm 0.020)(\log P - 1) - 6.213 \pm 0.005 \\
W_B^{BK}\,(0.050) &= (-3.691 \pm 0.018)(\log P - 1) - 5.913 \pm 0.005 \\
W_V^{VI}\,(0.068) &= (-3.614 \pm 0.025)(\log P - 1) - 5.935 \pm 0.007
\end{aligned}
$$

5.1 Gold Dataset based Wesenheit Leavitt Law

From the initial sample of 109 Cepheids, a gold dataset of 76 stars is selected by filtering based on photometric quality and their positions in the residual–correlation diagram. From this, Leavitt Laws are:

$$M_B\,(0.046) = (-1.885 \pm 0.020)(\log P - 1) - 3.102 \pm 0.005$$
$$M_V\,(0.036) = (-2.281 \pm 0.016)(\log P - 1) - 3.911 \pm 0.004$$
$$M_I\,(0.035) = (-2.581 \pm 0.015)(\log P - 1) - 4.691 \pm 0.004$$
$$M_J\,(0.017) = (-2.799 \pm 0.007)(\log P - 1) - 5.177 \pm 0.002$$
$$M_H\,(0.016) = (-2.931 \pm 0.007)(\log P - 1) - 5.552 \pm 0.002$$
$$M_K\,(0.004) = (-2.981 \pm 0.002)(\log P - 1) - 5.613 \pm 0.001$$
$$W_V^{VJ}\,(0.021) = (-3.018 \pm 0.009)(\log P - 1) - 5.710 \pm 0.003$$

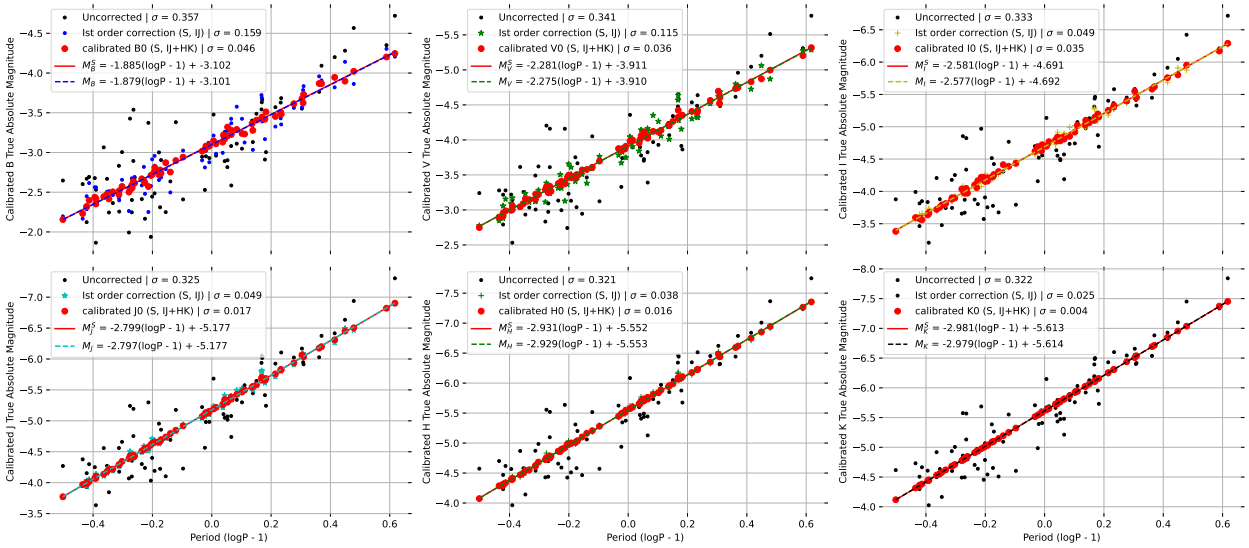

Figure 15: Calibrated $BVIJHK$ Leavitt Law based on 76 Galactic Cepheids (IRSB). First order distance correction made with infrared wesenheit (I - J). Tight red scatter in each plot represents second order calibrated Leavitt Law improving reddening correction with (H - K) wesenheit.

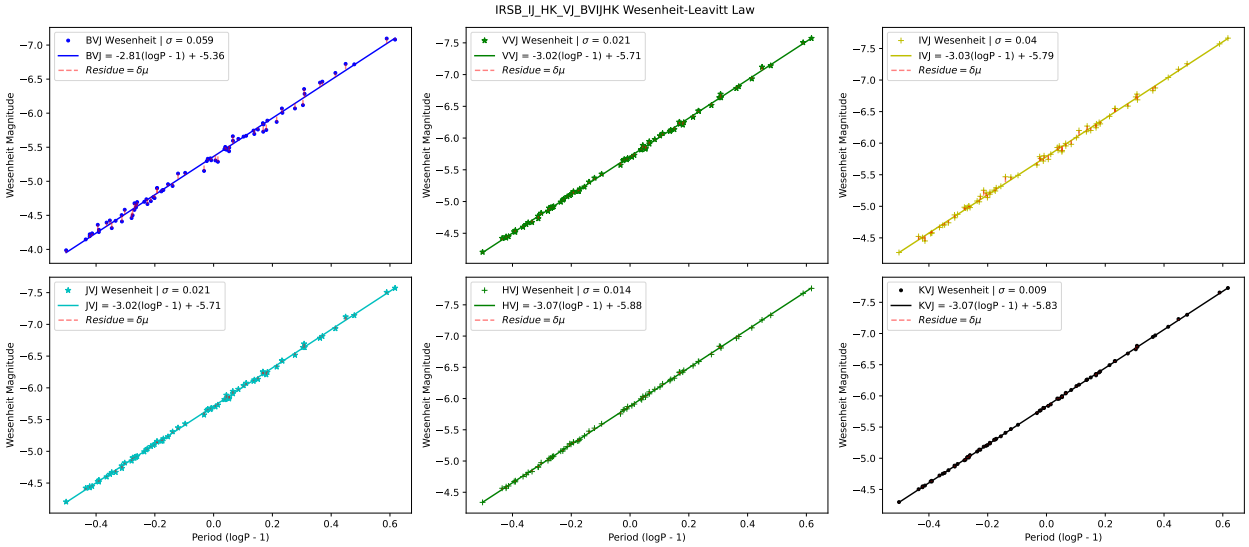

Figure 16: Calibrated $BVIJHK$ Wesenheit Leavitt Law shown here for (V-J) color.

5.2 Cross Validation with Cruz Cluster Cepheids

In the dataset, 17 Cepheids are identified as members of clusters with statistical parallaxes measured by Cruz Reyes et al. (2023). A comparison between the calibrated distances of these Cepheids shows a good agreement in reddening value with $\sigma = 0.049$.

For distance modulus, nine of 17 cluster Cepheid deviated by 0.1 mag only, but five Cepheids (EV Sct, QZ Nor, SV Vul, Y Sct and X Lac) have deviation larger than 0.4 mag.

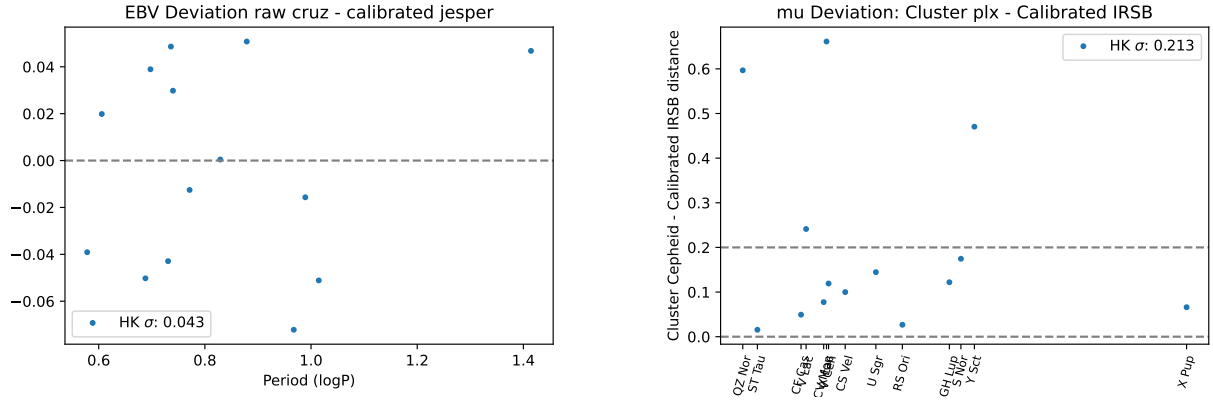

(a) Reddening correction comparision (b) Distance modulus comparision

Figure 17: Deviation of distance and reddening with 17 Cluster Cepheids (Cruz, 2023)

5.3 Cross Validation with Gaia parallax

Gaia parallax based distances are independent of reddening error as the method is fundamentally geometrical in nature. Although, Cepheid being one of the brightest target in the sky, leading to saturation of photons on the CCD causing a strong bais for longer period Cepheids. This makes parallax of Cepheid slightly uncertain as compare to dimmer stars. I have implimented the calibration algorithm on the same set of stars and determine calibrated distance for individual Cepheid. If the algorithm works perfectly, calibrated distance must agree with IRSB based calibrated distance.

6. Distance to Magellanic Clouds

In the vicinity of the Magellanic Clouds, several Cepheids are located, a subset of which have available VIJK photometry and estimated reddenings. For these stars, I adopt the extinction law from Wang & Chen (2023) for both the LMC and SMC, as summarized in Table 1, with R_V values of 3.4 and 2.53, respectively. The sample includes 29 Cepheids in the LMC and 32

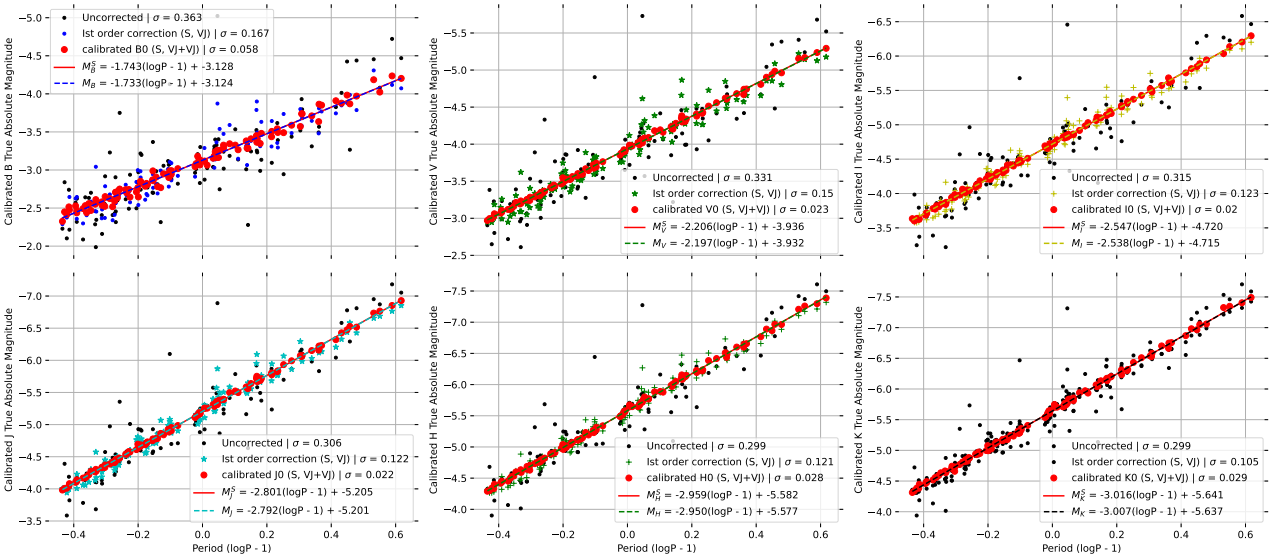

(a) Gaia parallax based Leavitt Law Calibration I: (I-H) and II: (V-J)

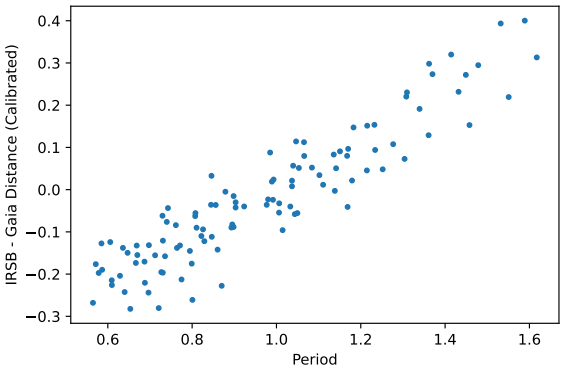

(b) IRSB-Gaia modulus Deviation

Figure 18: Deviation of distance and reddening with 17 Cluster Cepheids (Cruz, 2023)

in the SMC. Their calibrated Leavitt Law are as follows: Left - LMC and Right - SMC

$$V = (-2.707 \pm 0.101)(\log P - 1) + 14.296 \pm 0.041 \quad (16)$$

$$V = (-2.861 \pm 0.139)(\log P - 1) + 15.172 \pm 0.055 \quad (20)$$

$$I = (-2.960 \pm 0.076)(\log P - 1) + 13.605 \pm 0.030 \quad (17)$$

$$I = (-3.089 \pm 0.102)(\log P - 1) + 14.367 \pm 0.040 \quad (21)$$

$$J = (-3.124 \pm 0.056)(\log P - 1) + 13.216 \pm 0.022 \quad (18)$$

$$J = (-3.016 \pm 0.088)(\log P - 1) + 13.798 \pm 0.034 \quad (22)$$

$$K = (-3.226 \pm 0.043)(\log P - 1) + 12.783 \pm 0.017 \quad (19)$$

$$K = (-3.260 \pm 0.071)(\log P - 1) + 13.367 \pm 0.028 \quad (23)$$

(23)

Comparing the intercepts with Galactic Leavitt Law in each band yields distance moduli of 18.365 ± 0.110 for the LMC and 19.068 ± 0.038 for the SMC when the $VIJK$ bands are analyzed jointly.

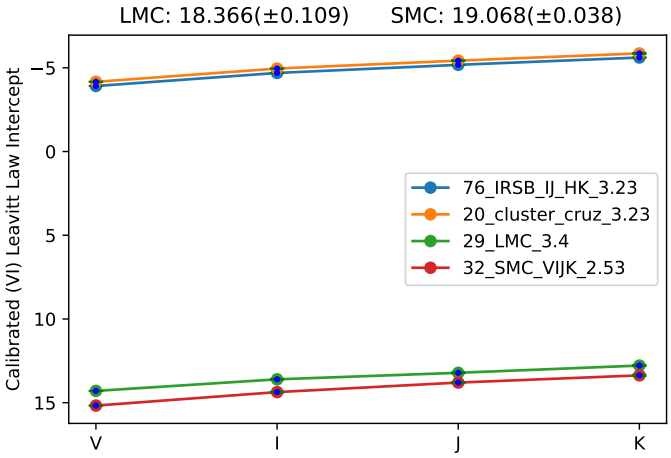

Figure 19: LMC and SMC distance using calibrated VIJK Leavitt Law intercepts

References

Cruz Reyes, N., Anderson, R. I., Zinn, J. C., Casertano, S., & Riess, A. G. (2023). Cluster cepheids: Improved distances from gaia edr3 and open cluster membership. *Astronomy & Astrophysics*, 672, A75. https://doi.org/10.1051/0004-6361/202244955

Fernie, J. D. (1995). Cepheid reddenings and the intrinsic colours of classical cepheids. *Information Bulletin on Variable Stars*, (4148), 1.

Fouqué, P., Arriagada, P., Storm, J., Barnes, T. G., Nardetto, N., Mérand, A., Kervella, P., Gieren, W., Benedict, G. F., & McArthur, B. (2007). A new calibration of galactic cepheid period-luminosity relations from b to k bands, and a 0.1 distance to the lmc. *Astronomy & Astrophysics*, 476(1), 73–81. https://doi.org/10.1051/0004-6361:20077611

Gaia Collaboration. (2023). Gaia data release 3: Summary of the contents and survey properties. *Astronomy & Astrophysics*, 674, A1.

Madore, B. F. (1982). The period-luminosity relation. iv-intrinsic relations and reddenings for the large magellanic cloud cepheids. *Astrophysical Journal, Part 1, vol. 253, Feb. 15, 1982, p. 575-579. Research supported by the Natural Sciences and Engineering Research Council of Canada, University of Toronto, and Science Research Council of England.*, 253, 575–579.

Madore, B. F., Freedman, W. L., & Moak, S. J. (2017). A method for improving galactic cepheid reddenings and distances. *The Astrophysical Journal*, 842(1), 42. https://doi.org/10.3847/1538-4357/aa71a0

Sandage, A., Tammann, G. A., & Reindl, B. (2004). New period–color and period–luminosity relations for the cepheid variables and the determination of the hubble constant. *Astronomy & Astrophysics*, 424, 43–84. https://doi.org/10.1051/0004-6361:20041231

Storm, J., et al. (2011). A new calibration of galactic cepheid period-luminosity relations from irsb method. *Astronomy & Astrophysics*, 534, A95. https://doi.org/10.1051/0004-6361/201117096

Wang, S., & Chen, X. (2023). Revisiting the extinction law of the magellanic clouds. *The Astrophysical Journal*, 951(1), 92. https://doi.org/10.3847/1538-4357/acd8da